Research Article

Muhammad Ramzan, Ebrahem A. Algehyne, Anwar Saeed*, Abdullah Dawar, Poom Kumam*, and Wiboonsak Watthayu

# Homotopic simulation for heat transport phenomenon of the Burgers nanofluids flow over a stretching cylinder with thermal convective and zero mass flux conditions

https://doi.org/10.1515/ntrev-2022-0089
received January 11, 2022; accepted March 15, 2022

**Abstract:** This study is focused to elaborate on the effect of heat source/sink on the flow of non-Newtonian Burger nanofluid toward the stretching sheet and cylinder. The current flow analysis is designed in the form of higher order nonlinear partial differential equations along with convective heat and zero mass flux conditions. Suitable similarity transformations are used for the conversion of higher order nonlinear partial differential equations into the nonlinear ordinary differential equations. For the computation of graphical and tabular results, the most powerful analytical technique, known as the homotopy analysis method, is applied to the resulting higher order nonlinear ordinary differential equations. The consequence of distinct flow parameters on the Burger nanofluid velocity, temperature, and concentration profiles are determined and debated in a graphical form. The key outcomes of this study are that the Burger nanofluid parameter and Deborah number have reduced the velocity of the Burger nanofluid for both the stretching sheet and cylinder. Also, it is attained that the Burger nanofluid temperature is elevated with the intensifying of thermal Biot number for both stretching sheet and cylinder. The Burger nanofluid concentration becomes higher with the escalating values of Brownian motion parameter and Lewis number for both stretching sheet and cylinder. The Nusselt number of the Burger nanofluid upsurges due to the increment of thermal Biot number for both stretching sheet and cylinder. Also, the different industrial and engineering applications of this study were obtained. The presented model can be used for a variety of industrial and engineering applications such as biotechnology, electrical engineering, cooling of devices, nuclear reactors, mechanical engineering, pharmaceutical science, bioscience, medicine, cancer treatment, industrial-grid engines, automobiles, and many others.

**Keywords:** Burger nanofluid, heat transfer, stretching cylinder, homotopy analysis method

*** Corresponding author: Anwar Saeed,** Center of Excellence in Theoretical and Computational Science (TaCS-CoE), Science Laboratory Building, Faculty of Science, King Mongkut's University of Technology Thonburi (KMUTT), 126 Pracha-Uthit Road, Bang Mod, Thung Khru, Bangkok 10140, Thailand, e-mail: anwarsaeed769@gmail.com
*** Corresponding author: Poom Kumam,** KMUTT Fixed Point Research Laboratory, Room SCL 802 Fixed Point Laboratory, Science Laboratory Building, Department of Mathematics, Faculty of Science, King Mongkut's University of Technology Thonburi (KMUTT), Bangkok 10140, Thailand; Center of Excellence in Theoretical and Computational Science (TaCS-CoE), Science Laboratory Building, Faculty of Science, King Mongkut's University of Technology Thonburi (KMUTT), 126 Pracha-Uthit Road, Bang Mod, Thung Khru, Bangkok 10140, Thailand; Department of Medical Research, China Medical University Hospital, China Medical University, Taichung 40402, Taiwan, e-mail: poom.kum@kmutt.ac.th
**Muhammad Ramzan, Wiboonsak Watthayu:** KMUTT Fixed Point Research Laboratory, Room SCL 802 Fixed Point Laboratory, Science Laboratory Building, Department of Mathematics, Faculty of Science, King Mongkut's University of Technology Thonburi (KMUTT), Bangkok 10140, Thailand; Center of Excellence in Theoretical and Computational Science (TaCS-CoE), Science Laboratory Building, Faculty of Science, King Mongkut's University of Technology Thonburi (KMUTT), 126 Pracha-Uthit Road, Bang Mod, Thung Khru, Bangkok 10140, Thailand
**Ebrahem A. Algehyne:** Department of Mathematics, Faculty of Science, University of Tabuk, P.O. Box 741, Tabuk 71491, Saudi Arabia; Nanotechnology Research Unit (NRU), University of Tabuk, Tabuk 71491, Saudi Arabia
**Abdullah Dawar:** Department of Mathematics, Abdul Wali Khan University, Mardan, 23200, Khyber Pakhtunkhwa, Pakistan

## Nomenclature

| | |
|---|---|
| $(r, \theta, z)$ | cylindrical polar coordinate |
| $(u, 0, w)$ | velocity components |

| | |
|---|---|
| $l$ | specific length |
| $T$ | fluid temperature |
| $C$ | fluid concentration |
| $T_w$ | surface temperature |
| $T_\infty$ | ambient temperature |
| $C_\infty$ | ambient temperature |
| $\lambda_1$ | relaxation time parameter |
| $\lambda_2$ | burger fluid material parameter |
| $\lambda_3$ | retardation time parameter |
| $\alpha_1$ | thermal diffusion coefficient |
| $k$ | thermal conductivity |
| $D_B$ | Brownian diffusivity |
| $\nu$ | kinematics viscosity |
| $Q_0$ | heat source/sink parameter |
| $\rho$ | fluid density |
| $C_p$ | specific heat at a constant pressure |
| $D_T$ | thermophoresis coefficient |
| $h_f$ | heat convection coefficient |

## Dimensionless symbols

| | |
|---|---|
| $\gamma$ | fluid curvature parameter |
| $\beta_1$ and $\beta_3$ | Deborah numbers |
| Pr | Prandtl number |
| $\beta_2$ | Burger fluid parameter |
| $\delta$ | dimensionless heat source/sink parameter |
| $Le$ | Lewis number |
| $Nt$ | thermophoresis parameter |
| $Nb$ | Brownian motion parameter |
| Re | Reynolds number |
| $Nu_z$ | Nusselt number |
| $Sh_z$ | local Sherwood number |
| $Bi$ | thermal Biot number |

## 1 Introduction

The non-Newtonian fluid research has become increasingly popular as a result of its importance and wide range of applications in industries and engineering systems like geophysical development, petrochemical advances, process design system, cooling and heating process, biomedical engineering, chemical engineering, metal processing, foodstuff, and oil reservoir engineering. Because of its widespread applications in engineering and industry, researchers and scientists emphasized their research on the non-Newtonian nanofluid problem. Khan *et al.* [1] addressed the significance of Dufour and Soret parameters on the flow of non-Newtonian micropolar liquid toward the exponential nonlinear stretching cylinder in which they found that Reynolds number diminished the thickness of the micropolar liquid. Bilal *et al.* [2] explained the performance of activation energy on the flow of non-Newtonian Casson nanoliquid under the rotating thin needle. They inspected that the nanoliquid concentration is enhanced with the increment of activation energy. Ramzan *et al.* [3] designed the model of non-Newtonian nanoliquid in the existence of entropy and dipole effects on the thin needle. Their conclusions showed that the ferromagnetic parameter enhanced the nanofluid velocity. Alhadihrami *et al.* [4] considered the study of non-Newtonian Casson liquid through the occurrence of heat transfer and porosity effect in a porous medium. They attained that the transfer of heat is improved when the porosity parameter is higher. Mallawi *et al.* [5] designated the modeling of non-Newtonian liquid above the Riga plate with the influence of Cattaneo-Christov heat flux. They studied that the thickness of thermal boundary layer of viscoelastic liquid is higher than the second-grade fluid. Dawar *et al.* [6] examined the impacts of non-isosolutal and non-isothermal conditions over the flow of Williamson nanofluid above the wedge or cone. For the explanation of their problem, they employed the homotopy analysis method (HAM) on the higher order nonlinear ordinary differential equations (ODEs). Reddy *et al.* [7] explored the consequence of chemical reaction on the three-dimensional magnetohydrodynamic (MHD) flow of non-Newtonian Maxwell nanoliquid through the stretched surface and examined that the radiation parameter weakened the nanoliquid temperature. Qaiser *et al.* [8] presented the significance of mass transfer and thermal radiation on the non-Newtonian mixed convection flow of Walter-B nanoliquid under the stretchable sheet. Their fallouts show that the Brownian motion parameter improved Sherwood number.

Nanofluids are fluids that contain suspended nanoparticles that are less than a hundred nanometers in size and are used to improve thermal conductivity. The study of nanofluid has attracted the attention of researchers and scientists due to its vast variety of applications in the technical and industrial fields. The industrial and engineering applications of the nanofluid are heat exchangers, vehicle cooling, electronic device cooling, nuclear reactors, transformer cooling, vehicle thermal management, *etc.* The nanofluid is also used in medical treatments such as wound treatment, resonance imaging, and cancerous and noncancerous tumor treatment. That is why researchers and scientists used nanofluid in their

experiments. Hiba *et al.* [9] computed the mathematical modeling of MHD flow of hybrid nanofluid with Ag–MgO as the nanoparticle and water as the base fluid and adopted the Galerkin finite element method for the numerical solution of their problem. Ouni *et al.* [10] presented the influence of thermal radiation on the flow of hybrid nanofluid toward the parabolic solar collector in the presence of solar radiation. They examined that hybrid nanofluid temperature is higher for thermal radiation parameters. Khan *et al.* [11] demonstrated the MHD flow of three-dimensional cross nanofluid by applying Soret and Dufour numbers in which they found that Soret number raised the rate of heat transport. Bejawada *et al.* [12] explained the problem of MHD flow of nanofluid with the occurrence of viscous dissipation and chemical reaction toward the inclined plate. In this work, it was noted that the concentration of the nanofluid was declined for Schmidt number. Jamshed *et al.* [13] inspected the consequence of the Joule heating effect on the MHD flow of tangent hyperbolic hybrid nanofluid under the stretching plate. Their problem is simulated numerically with the application of the Keller box scheme. Redouane *et al.* [14] scrutinized the MHD flow of hybrid nanofluid over the rotating cylinder through the existence of entropic generation. From this examination, it was observed that the entropy generation of the hybrid nanofluid increased with the rising of porosity parameters. Waqas *et al.* [15] evaluated the consequence of nonlinear thermal radiation over the flow of nanofluid in a permeable cylinder. From this study, they determined that the higher estimation of Reynolds number weakened the velocity of the nanoliquid. Hayat *et al.* [16] scrutinized the convective flow of Jeffrey nanoliquid through the stretchable cylinder along with heat transport behavior. They examined that Schmidt number diminished the nanofluid concentration. Siddiqui *et al.* [17] evaluated the problem of boundary layer MHD flow of two-dimensional Maxwell nanoliquid with the incidence of viscous dissipation through the melting surface. From this observation, they noted that the porosity of the nanofluid improved the entropy. Awan *et al.* [18] computed the mathematical solution of the micropolar nanofluid model with the assistance of the Runge-Kutta method through the presence of Hall current and MHD between the two parallel plates and also discussed some important physical properties of nanofluid. Ramesh *et al.* [19] reported the consequence of slip and suction/injection effects on the flow of Casson-micropolar nanoliquid under the two-rotating disks in which the reduction in the rate of heat and mass transportation is perceived for the Brownian motion parameter. Lv *et al.* [20] checked the behavior of entropy and Cattaneo–Christov heat flux over the spinning disk in the flow of bioconvection Reiner–Rivlin nanofluid and their concluding remarks showed that a greater estimation of Lewis and Peclet numbers decrease the motile gyrotactic microorganism profile of the nanoliquid. Waqas *et al.* [21] detected the movement of heat source/sink on the three-dimensional bioconvection flow of Carreau nanoliquid over the stretchable surface. From this study, they explained that the temperature of the nanofluid is raised for heat source/sink and Biot parameters. Kumar *et al.* [22] stated the role of Darcy–Forchheimer and heat transport on the flow of stagnation region nanofluid over the flat sheet. Form this study, they noticed the relationship between heat transfer and the Dacry–Forchheimer parameter. Other studies related to the nanofluid flow problem can be found in the references [23–25].

From the last few decades, scientists and researchers have shown a keen interest in studying the MHD flow problems due to its vast array of applications in the arena of engineering and industries. The MHD is a branch of physical science that studies magnetic and electrical fluid behavior such as plasma, liquid metals, electrolytes, and saltwater. In engineering and industry, the MHD has a broad array of applications, especially in the field of biomedical science such as blood flows, tissue temperature, MHD power plants, cell separation, MHD generators, and treatment of tumors. Shah *et al.* [26] examined the MHD flow of nanofluid along with energy flux due to concentration gradient, mass flux, and temperature gradient toward the horizontal surface and employed the finite difference code (Matlab Function) (bvp4c) technique for the evaluation of the numerical solution of their problem. Wakif *et al.* [27] presented the MHD mixed convective flow of radiative Walter-B fluid through the inclusion of Fourier's and Fick's laws under the linear stretching surface. From this analysis, it is noticed that the amplification in the magnetic field parameter led to the amplification of nanofluid velocity. Shafiq *et al.* [28] reported the MHD flow of Casson Water/Glycerin nanofluid in the presence of Darcy-Forchheimer over the rotating disk and detected that the skin friction coefficient is enhanced with the increment of the Darcy–Forchheimer parameter. Wakif *et al.* [29] scrutinized the combined effects of Joule heating and wall suction on the MHD flow of viscous by electrically conducting fluid over the Riga plate. They obtained that the rate of heat transport is augmented with the augmentation of wall suction of the fluid. Wakif *et al.* [30] inspected the presence of thermal conductivity and temperature-dependent viscosity on the MHD flow of Casson fluid toward the horizontal stretching sheet under the convective conditions. In this inquiry, it is notable that the fluid Casson parameter decayed the surface drag force. Wakif [31] used the spectral local linearization method for

the numerical investigation of MHD flow of Walter-B fluid along with the gyrotactic microorganism behavior and attained that the Lorentz force weakened the Nusselt number of the fluid. Khashi'ie *et al.* [32] observed the Joule heating effect on the MHD boundary layer flow of hybrid nanoliquid above the moving plate. From their numerical result, it was noted that the magnetic and suction parameters augmented the heat rate transport. Krishna *et al.* [33] explored the mathematical modeling of MHD flow of Ag–Tio/$H_2O$ Casson hybrid nanoliquid in a porous medium along with the exponential vertical sheet in which Ag–Tio are the nanoparticles and water was taken as a base liquid. Haider *et al.* [34] inspected the significance of thermal radiation and activation energy on the unsteady MHD flow of nanoliquid past a stretchable surface. From tthis inquiry, they distinguished that the nanoparticle volume fraction of the nanofluid upsurges with the rise of activation energy. Ahmed *et al.* [35] explained the computation assessment of thermal conductivity on the MHD flow of Williamson nanoliquid along with the heat transport effect over the exponentially curved surface. They employed the bvp4c technique for the numerical description of the problem. In another study of MHD, Tassaddiq [36] conducted the study of MHD flow of hybrid micropolar nanoliquid with the occurrence of Cattaneo-Christov heat flux and found that the thermal profile of the hybrid nanofluid is raised against micropolar parameter. Qayyum *et al.* [37] addressed the Newtonian heat and mass conditions on the modeling of MHD flow of Walter-B nanoliquid along the stretched sheet. From this study, they found that the relation between local Nusselt and Sherwood numbers is reverse for thermophoresis parameter. Ghasemi and Hatami [38] scrutinized the presence of solar radiation over the MHD stagnation point flow of nanoliquid under the stretchable surface. From this scrutiny, they observed that the temperature of the nanofluid is higher for the solar radiation parameters. Ramzan *et al.* [39] reviewed the MHD flow of nanoliquid through the occurrence of homogeneous and heterogeneous reaction effects under the rotating disk. From this study, it was noted that the dimensionless constant of the rotating disk boosted the homogeneous/heterogeneous reactions profile of the nanofluid.

Heat and mass transport phenomena have recently found an extensive variety of applications in engineering and industry such as industrial equipment, rotating machinery, aerospace, power generation, chemical, and material processes, automotive, food processing, plastics, petrochemical, poultry further processing, rubbers aircraft engine cooling, and environmental control system. Because of the aforementioned applications, scientists and researchers have focused their research on heat and mass transport phenomena. Awais *et al.* [40] elaborated on the result of gyrotactic microorganisms over the MHD flow of bio nanofluid having the heat and mass transport features. From their outcomes, they detected that the bioconvection Rayleigh number and convection parameter elevated the rate of heat and mass transport. Srinivasulu and Goud [41] described the combined influence of heat and mass transport over the flow of Williamson nanoliquid due to the stretched sheet. They found the aspect of different flow parameters on the nanofluid velocity, temperature, and concentration. Zeeshan *et al.* [42] elaborated the study of MHD flow of nanoliquid over the vertical wavy sheet with the existence of heat and mass transfer and applied the Keller-box scheme for the numerical evolution of their problem. Punith Gowda *et al.* [43] explicated the heat and mass transport behavior on the Marangoni driven boundary layer flow of non-Newtonian nanoliquid with chemical reaction along the rectangular surface. In their study, they noticed that the porosity parameter decayed the nanofluid Nusselt number. Shi *et al.* [44] considered the exponential stretching surface for the explanation of three-dimensional MHD flow of radiative Maxwell nanoliquid along with the occurrence of heat and mass transfer effects. In this study, they discussed that the nanofluid velocity reduces as the rotation parameter upsurges. Zhao *et al.* [45] talked about the stagnation point flow of a tangent hyperbolic nanoliquid with the assumption of heat and mass transmission and entropy behavior. From this study, they deliberated that the enhancing estimation of the Brownian motion parameter boosted the entropy of the nanofluid. Arif *et al.* [46] conducted the occurrence of heat and mass transport on the modeling of Casson liquid along with ramped wall temperature in which $MoS_2$–GO are the nanoparticles and engine oil is taken as a base liquid. Rasool *et al.* [47] reported the flow analysis of convective MHD nanofluid with the perception of heat and mass transfer in a stretchable surface. Their study explained that the concentration of the nanofluid is the growing function of the porosity parameter.

As a result of the above-mentioned literature, it was perceived that no consideration was given to studying the influence of heat source/sink effect on the flow of Burger nanofluid earlier. To fill this gap, the Burger nanofluid along with convective boundary conditions in the presence of Brownian and thermophoresis diffusion was taken into the interpretation. In the current analysis, the physical situation was being modeled in the form of stretching cylinder (see Figure 1). From Figure 1, the present physical situation explained that when curvature parameter ($\gamma = 0$) then physically, the current flow problem is for stretching sheet, but when ($\gamma > 0$) then the current flow problem is for stretching cylinder. The role of

zero mass flux conditions in the Burger nanofluid problem is that there are no mass flux nanoparticles which mean that the nanoparticles' mass flux is assumed to be zero on the surface, and that is why the current model is taken with zero mass flux condition (see Wakif *et al.* [48]). This work is very useful in different areas of engineering and industrial fields such as nuclear reactors, cooling of devices, plastics manufacturing, paper production, food processing, glass blowing, and synthetics fibers. The resultant higher orders nonlinear ODEs were resolved by the exploitation of HAM. The consequence of various flow parameters on the velocity, temperature, and concentration of Burger nanofluid was investigated in the graphical form. Also, the Nusselt number of Burger nanofluid was presented in a tabular form and discussed in detail.

## 2 Problem formulation

Consider the steady and incompressible flow of Burger nanofluid problem over a stretching cylinder with heat source/sink effect. $r$, $\theta$, and $z$ are the cylindrical coordinates in which $u$ is the velocity component along the $r$-axis and $w$ is the velocity component along the $z$-axis. The stretching velocity of the cylinder is $w(z) = \frac{U_0 z}{l}$ in which $z$ is used as the reference velocity, while $l$ is the specific length. $T$, $T_w$, and $T_\infty$ are the temperature, temperature at the surface, and ambient temperature, respectively. $C$ and $C_\infty$ are the concentration and ambient concentration, respectively. In addition, the effect of convective heat and zero mass flux conditions were taken. The geometrical representation of the flow problem is displayed in Figure 1.

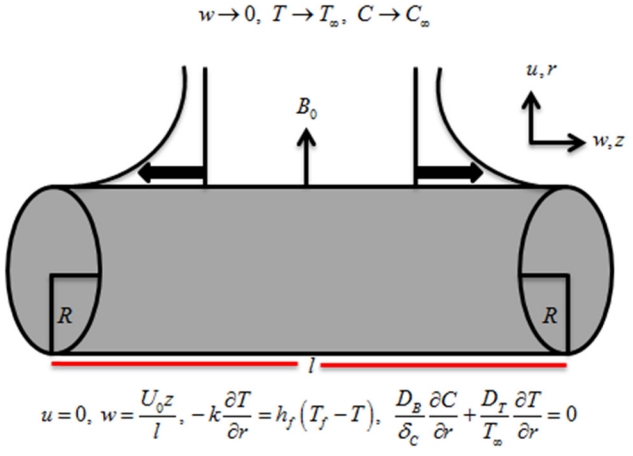


**Figure 1:** Geometry of the flow problem.

In view of the above assumptions, the leading equations of the current analysis are deliberated as [49–51]:

$$\frac{\partial u}{\partial r} + \frac{u}{r} + \frac{\partial w}{\partial z} = 0, \tag{1}$$

$$\begin{aligned} &u\frac{\partial w}{\partial r} + w\frac{\partial w}{\partial z} + \lambda_1\left(u^2\frac{\partial^2 w}{\partial r^2} + w^2\frac{\partial^2 w}{\partial z^2} + 2uw\frac{\partial^2 w}{\partial z \partial r}\right) \\ &+ \lambda_2\left[2u^2\left(\frac{\partial u}{\partial r}\frac{\partial^2 w}{\partial r^2} + \frac{\partial w}{\partial r}\frac{\partial^2 w}{\partial r \partial z}\right)\right. \\ &\times u^3\frac{\partial^3 w}{\partial r^3} + w^3\frac{\partial^3 w}{\partial z^3} - u^2\left(\frac{\partial w}{\partial r}\frac{\partial^2 u}{\partial r^2} + \frac{\partial w}{\partial z}\frac{\partial^2 w}{\partial r^2}\right) \\ &+ 2w^2\frac{\partial u}{\partial z}\frac{\partial^2 w}{\partial r \partial z} + w^2\left(\frac{\partial w}{\partial z}\frac{\partial^2 w}{\partial z^2} - \frac{\partial w}{\partial r}\frac{\partial^2 u}{\partial z^2}\right) \\ &+ 3uw\left(u\frac{\partial^3 w}{\partial r^2 \partial z} + w\frac{\partial^3 w}{\partial z^2 \partial r}\right) + 2uw\left(\frac{\partial u}{\partial r}\frac{\partial^2 w}{\partial z \partial r} + \frac{\partial u}{\partial z}\frac{\partial^2 w}{\partial r^2}\right. \\ &\left.\left. + \frac{\partial w}{\partial r}\frac{\partial^2 w}{\partial z^2} - \frac{\partial w}{\partial r}\frac{\partial^2 u}{\partial r \partial z}\right)\right] \\ &= \nu\left(\frac{\partial^2 w}{\partial r^2} + \frac{1}{r}\frac{\partial w}{\partial r}\right)\nu\lambda_3\left[u\frac{\partial^3 w}{\partial r^3} + w\frac{\partial^3 w}{\partial r^2 \partial z}\right. \\ &+ \frac{u}{r}\frac{\partial^2 w}{\partial r^2} - \frac{\partial w}{\partial r}\frac{\partial^2 u}{\partial r^2} + \frac{w}{r}\frac{\partial^2 w}{\partial r \partial z} \\ &\left. - \frac{1}{r}\frac{\partial u}{\partial r}\frac{\partial w}{\partial r} - \frac{1}{r}\frac{\partial w}{\partial r}\frac{\partial w}{\partial z} - \frac{\partial w}{\partial z}\frac{\partial^2 u}{\partial r^2}\right], \end{aligned} \tag{2}$$

$$\begin{aligned} u\frac{\partial T}{\partial r} + w\frac{\partial T}{\partial z} &= \alpha_1\frac{1}{r}\left(\frac{\partial}{\partial r}\left(r\frac{\partial T}{\partial r}\right)\right) \\ &+ \tau\left[\frac{D_B}{\delta_C}\frac{\partial C}{\partial r}\frac{\partial T}{\partial r} + \frac{D_T}{T_\infty}\left(\frac{\partial T}{\partial r}\right)^2\right] \\ &+ \frac{Q_0(T - T_\infty)}{\rho C_p}, \end{aligned} \tag{3}$$

$$\begin{aligned} &u\frac{\partial C}{\partial r} + w\frac{\partial C}{\partial z} \\ &= D_B\frac{1}{r}\left(\frac{\partial}{\partial r}\left(r\frac{\partial C}{\partial r}\right)\right) + \frac{\delta_C D_T}{T_\infty}\frac{1}{r}\left(\frac{\partial}{\partial r}\left(r\frac{\partial T}{\partial r}\right)\right), \end{aligned} \tag{4}$$

with boundary conditions:

$$\left\{\begin{array}{l} u = 0,\ w = \dfrac{U_0 z}{l},\ -k\dfrac{\partial T}{\partial r} = h_f(T_w - T), \\ \dfrac{D_B}{\delta_C}\dfrac{\partial C}{\partial r} + \dfrac{D_T}{T_\infty}\dfrac{\partial T}{\partial r} = 0 \text{ at } r = R, \\ w \to 0,\ T \to T_\infty,\ C \to C_\infty \text{ as } r \to \infty. \end{array}\right\} \tag{5}$$

where $u$ and $w$ are the velocity components, $\lambda_1$ is the relaxation time, $\lambda_2$ is the material parameter of the Burger fluid, $\lambda_3$ is the retardation time, $T$ is the temperature of the nanofluid, $\alpha_1 = \frac{k}{\rho C_p}$ is the thermal diffusion coefficient in which $k$ is the thermal conductivity and $\rho C_p$ is the heat capacitance, $D_B$ is the diffusion coefficient, $\nu$ is the

kinematics viscosity, $Q_0$ the dimensional heat source/sink, the liquid density is $\rho$, $C_p$ is the specific heat, $D_T$ is the thermophoresis coefficient, and $h_f$ is the coefficient of heat convection.

The similarity transformations in the dimensionless form are [50,51]:

$$\begin{aligned} u &= -\frac{R}{r}\sqrt{\frac{U_0\nu}{l}}f(\xi),\ w = \frac{U_0 z}{l}f'(\xi),\\ \theta(\xi) &= \frac{T - T_\infty}{T_w - T_\infty},\ \phi(\xi) = \frac{C - C_\infty}{C_\infty},\\ \xi &= \sqrt{\frac{U_0}{\nu l}}\left(\frac{r^2 - R^2}{2R}\right). \end{aligned} \tag{6}$$

With the implementation of the above similarity variables defined in equation (6), the equation of continuity is satisfied and the dimensionless form of equations (2)–(4) are

$$\begin{aligned} &(1+2\gamma\xi)^3 f''' + (1+2\gamma\xi)^2\beta_1[2ff'f'' - f^2f'''] \\ &- (1+2\gamma\xi)\alpha\beta_1 f^2 f'' - 4\gamma^2\beta_2 f'''f'' - (1+2\gamma\xi)^2 \\ &\times \beta_2[3f^2(f'')^2 + 2f(f')^2 f'' - f^3 f''''] \\ &- 4\gamma\beta_3(1+2\gamma\xi)^2 ff''' + (1+2\gamma\xi)\gamma\beta_2[3f^2f'f'' + f^3f'''] \\ &+ (1+2\gamma\xi)^2[2\gamma f'' + ff'' - (f')^2] \\ &+ (1+2\gamma\xi)^3\beta_3[(f'')^2 - ff''''] = 0, \end{aligned} \tag{7}$$

$$\begin{aligned} &(1+2\gamma\xi)\theta'' + 2\gamma\theta' + \mathrm{Pr}f\theta' + \mathrm{Pr}\delta\theta \\ &+ \mathrm{PrN}b\phi'\theta'(1+2\gamma\xi) + \mathrm{PrN}t(\theta')^2(1+2\gamma\xi) = 0, \end{aligned} \tag{8}$$

$$\begin{aligned} &(1+2\gamma\xi)\phi'' + 2\gamma\phi' + \mathrm{LePr}f\phi' + (1+2\gamma\xi)\left(\frac{\mathrm{Nt}}{\mathrm{Nb}}\right)\theta'' \\ &+ 2\gamma\left(\frac{\mathrm{Nt}}{\mathrm{Nb}}\right)\theta' = 0, \end{aligned} \tag{9}$$

The boundary conditions in the dimensionless form are

$$\begin{bmatrix} f(0) = 0, f'(0) = 1,\ f'(\infty) = 0, \\ \theta'(0) = \mathrm{Bi}(\theta(0) - 1),\ \theta(\infty) = 0, \\ \mathrm{Nb}\phi'(0) + \mathrm{Nt}\theta'(0) = 0,\ \phi(\infty) = 0. \end{bmatrix}. \tag{10}$$

In the above equations, $\gamma\left(=\frac{1}{R}\sqrt{\frac{\nu l}{U_0}}\right)$ is the curvature parameter of the fluid, $\beta_1\left\{=\lambda_1\frac{U_0}{l}\right\}$ and $\beta_3\left\{=\lambda_3\frac{U_0}{l}\right\}$ are Deborah numbers, $\beta_2\left(=\lambda_2\left(\frac{U_0}{l}\right)^2\right)$ is the Burger fluid parameter, $\delta\left(=\frac{lQ_0}{U_0(\rho C_p)}\right)$ is the heat source/sink parameter, $\mathrm{Le}\left(=\frac{\alpha_1}{D_B}\right)$ is the Lewis number of the nanofluid, $\mathrm{Pr}\left(=\frac{\nu}{\alpha_1}\right)$ is the Prandtl number, $\mathrm{Nt}\left(=\frac{\tau D_T(T_w - T_\infty)}{\nu T_\infty}\right)$ is the thermophoresis parameter, $\mathrm{Nb}\left(=\frac{\tau D_B C_\infty}{\nu\delta_c}\right)$ is the Brownian motion parameter, and $B_i\left(=\frac{h_f}{k}\frac{R}{r}\sqrt{\frac{\nu l}{U_0}}\right)$ is the thermal Biot number.

The physical quantities including Nusselt number and local Sherwood number are defined as

$$\mathrm{Nu}_z = \frac{zq_m}{k(T_w - T_\infty)},\ \mathrm{Sh}_z = \frac{zj_w}{D_B(C_w - C_\infty)}. \tag{11}$$

The heat $q_m$ and mass flux $j_w$ is defined as

$$q_m = -k\left(\frac{\partial T}{\partial r}\right)_{r=R},\ j_w = -D_B\left(\frac{\partial C}{\partial r}\right)_{r=R}. \tag{12}$$

By applying the similarity transformations, the Sherwood number becomes zero and the Nusselt number reduces as

$$\mathrm{Nu}_z\,\mathrm{Re}^{-\frac{1}{2}} = -\theta'(0), \tag{13}$$

where $\mathrm{Re} = \frac{w(z)z}{\nu}$ is the local Reynolds number.

# 3 The solution to the problem

The HAM provides several advantages over other methods. Therefore, the present scheme is very useful for the analytical solution of the higher order nonlinear ODEs along with boundary conditions. The HAM method was used to solve the problem because it offers the following benefits:

1) Without linearization and discretization of nonlinear differential equations, the proposed technique is simulated for an accurate solution.
2) It is a more generalized method that works for both weakly and strongly nonlinear problems and is independent of small or large parameters.
3) The region and the rate of convergence of series solutions are controllable and adjustable with the help of HAM.
4) The HAM is free from rounding of errors and essay for computation.

That is why the HAM is preferable over other techniques due to the above-mentioned advantages. The linear operator and initial guesses are defined as

$$\begin{bmatrix} f_0(\eta) = 1 - e^{-\xi}, \\ \theta_0(\eta) = \frac{\mathrm{Bi}}{(1+\mathrm{Bi})}e^{-\xi}, \\ \phi_0(\eta) = -\frac{\mathrm{Nt}}{\mathrm{Nb}}\frac{\mathrm{Bi}}{(1+\mathrm{Bi})}e^{-\xi}, \end{bmatrix}, \tag{14}$$

$$\begin{Bmatrix} L_f = f''' - f', \\ L_\theta = \theta'' - \theta, \\ L_\phi = \phi'' - \phi, \end{Bmatrix}, \tag{15}$$

such that

$$\begin{Bmatrix} L_f[C_1 + C_2\exp(-\xi) + C_3\exp(\xi)] = 0, \\ L_\theta[C_4\exp(-\xi) + C_5\exp(\xi)] = 0, \\ L_\phi[C_6\exp(-\xi) + C_7\exp(\xi)] = 0. \end{Bmatrix}, \tag{16}$$

where $C_i (i = 1-7)$ are the arbitrary constants.

## 4 Convergence analysis of the homotopy solution

HAM is used to handle the series solutions of the simulated system of nonlinear differential equations. The auxiliary parameter $\hbar$ is used to manipulate and control the convergence areas of $f''(0)$, $\theta'(0)$, and $\phi'(0)$. Figures 2–4 are drawn to check the convergence region of $f''(0)$, $\theta'(0)$, and $\phi'(0)$. Finally, the convergence region of $f''(0)$, $\theta'(0)$, and $\phi'(0)$ are $-1.0 \le \hbar_f \le 1.0$, $-0.8 \le \hbar_\theta \le 0.8$, and $-0.75 \le \hbar_\phi \le 0.75$, respectively.

## 5 Validation

A comparison between the present results and the previously published results is demonstrated in Table 1. For the validation of the current problem from Table 1, it was noted that the current findings were in good consistency with previously published findings.

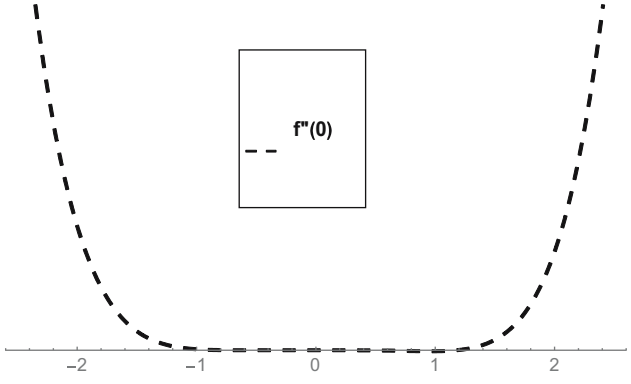


**Figure 2:** $h$-Curve for $f''(0)$.

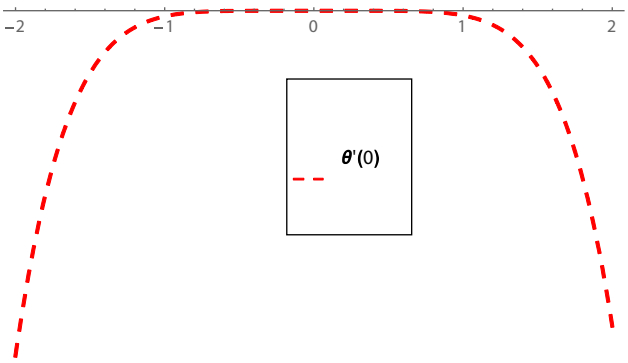


**Figure 3:** $h$-Curve for $\theta'(0)$.

**Table 1:** Analysis of the present results with previously published results

| Pr | $\frac{N u_z}{\sqrt{Re_r}}$ | | | | |
|---|---|---|---|---|---|
| | **Ref. [52]** | **Ref. [53]** | **Ref. [54]** | **Ref. [55]** | **Present results** |
| 0.07 | 0.0665 | 0.0656 | 0.0663 | 0.0656 | 0.0654 |
| 0.20 | 0.1691 | 0.1691 | 0.1691 | 0.1691 | 0.1691 |
| 0.70 | 0.4539 | 0.4539 | 0.4539 | 0.4539 | 0.4539 |
| 2.00 | 0.9114 | 0.9114 | 0.9113 | 0.9115 | 0.9114 |

## 6 Results and discussion

In Section 6, the analytical solution of the Burger nanofluid with convective heat and mass transport phenomena was discussed. For the physical computation of this study, the HAM was employed on the higher order nonlinear ODEs (6–8) along with boundary conditions (9). The significance of distinct flow parameters over the field of velocity, temperature, and concentration of the Burger nanofluid for both stretching sheet ($\gamma = 0$) and cylinder

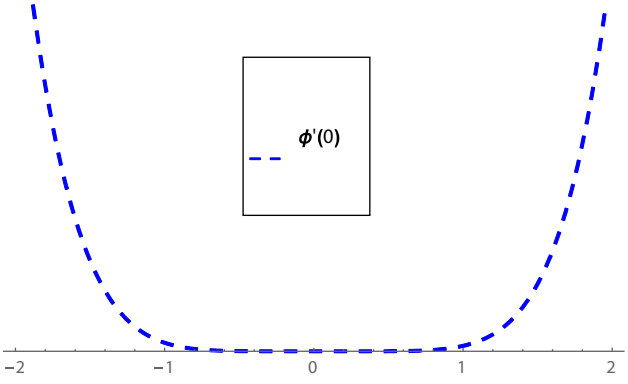


**Figure 4:** $h$-Curve for $\phi'(0)$.

**Table 2:** Effects of Bi and $\delta$ on $\mathrm{Nu}_z\,\mathrm{Re}^{-\frac{1}{2}}$ for $\gamma = 0$ and $\gamma > 0$

| Bi | $\delta$ | $\mathrm{Nu}_z\,\mathrm{Re}^{-\frac{1}{2}}$ for sheet ($\gamma = 0$) | $\mathrm{Nu}_z\,\mathrm{Re}^{-\frac{1}{2}}$ for cylinder ($\gamma > 0$) |
|---|---|---|---|
| 0.1 | | 0.080030 | 0.081705 |
| 0.2 | | 0.081965 | 0.083202 |
| 0.3 | | 0.148192 | 0.150276 |
| 0.4 | | 0.201516 | 0.204485 |
| | 0.2 | 0.211584 | 0.212713 |
| | 0.4 | 0.207679 | 0.208807 |
| | 0.6 | 0.203774 | 0.204902 |
| | 0.8 | 0.199868 | 0.200997 |

($\gamma > 0$) were computed in a graphical form. The ranges of all effective parameters were fixed in a graphical discussion, and only one parameter varies to plot their respective graph. The ranges of distinct flow parameters were $\beta_1 = 0.3$, $\beta_2 = 0.2$, $\beta_3 = 1.0$, $\delta = 1.3$, Bi = 0.3, Pr = 6.0, Le = 1.0, Nb = 0.2, and Nt = 1.0. Also, the Nusselt number $\mathrm{Nu}_z$ against flow parameters for both the stretching sheet ($\gamma = 0$) and cylinder ($\gamma > 0$) were calculated and discussed in detail.

## 6.1 Table discussion

Table 2 is made to check the effects of various flow parameters such that Biot number Bi, and heat generation parameter $\delta$ on the Nusselt number $\mathrm{Nu}_z\,\mathrm{Re}^{-\frac{1}{2}}$ of the Burger nanofluid for both stretching sheet ($\gamma = 0$) and cylinder ($\gamma > 0$). It was perceived that the Nusselt number $\mathrm{Nu}_z\,\mathrm{Re}^{-\frac{1}{2}}$ was higher for both stretching sheet ($\gamma = 0$) and cylinder ($\gamma > 0$) with the improvement of *Bi*. Also, it was observed that the expanding estimation of heat generation parameter $\delta$ reduced the Nusselt number for both the stretching sheet ($\gamma = 0$) and the stretching cylinder ($\gamma > 0$).

## 6.2 Velocity profile

Figures 5–7 display the effects of the Deborah number $\beta_1$, Burger nanofluid parameter $\beta_2$, and Deborah number $\beta_3$ for both stretching sheet ($\gamma = 0$) and cylinder ($\gamma > 0$). The variation in nanofluid velocity for higher estimation of Deborah number $\beta_1$ is described in Figure 5. From Figure 5, it was detected that with the increase of the Deborah number $\beta_1$, the Burger nanofluid velocity was reduced for both the stretching sheet ($\gamma = 0$) and cylinder ($\gamma > 0$). Deborah number was defined as the ratio between the relaxation time parameter and observation time

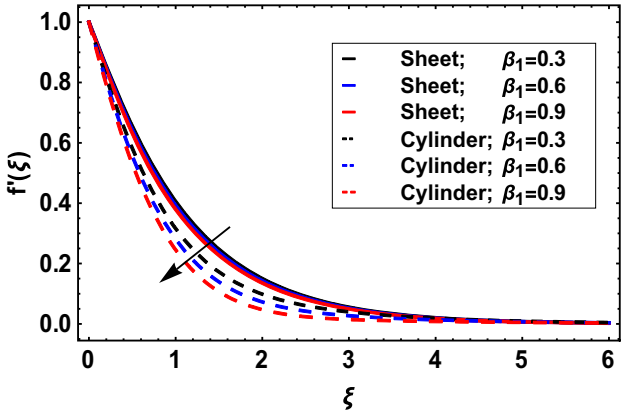


**Figure 5:** Change in nanofluid velocity due to $\beta_1$.

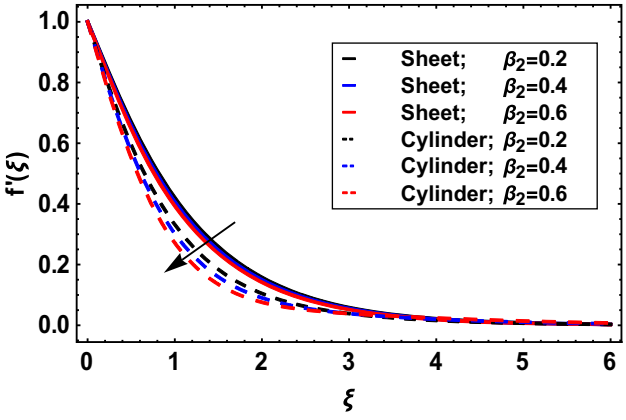


**Figure 6:** Change in nanofluid velocity due to $\beta_2$.

parameter. With the increment of Deborah number, the boundary layer thickness was reduced and the relaxation time parameter of the fluid was enlarged, that's why the Burger fluid velocity became lower. Also, in the fluid motion, the resistance became higher due to amplification

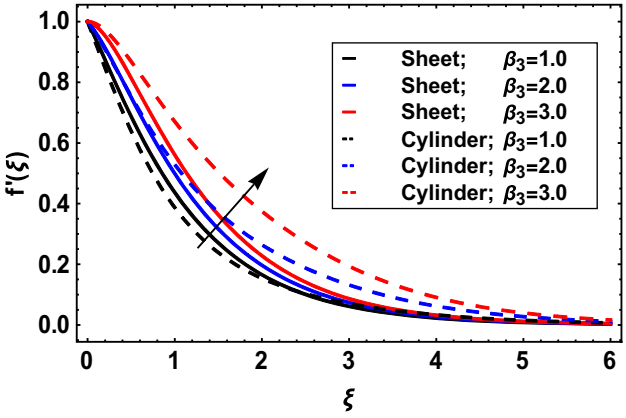


**Figure 7:** Change in nanofluid velocity due to $\beta_3$.

of the relaxation time parameter which led to diminishing Burger fluid velocity. Figure 6 illustrated the consequence of the Burger nanofluid parameter $\beta_2$ for both the stretching sheet ($\gamma = 0$) and cylinder ($\gamma > 0$) on the nanofluid velocity. From this study, it was perceived that the velocity of the Burger nanofluid for both the stretching sheet ($\gamma = 0$) and cylinder ($\gamma > 0$) was diminished for the Burger nanofluid parameter $\beta_2$. Similarly, the collision between the fluid particles was raised when the relaxation time parameter in terms of the Burger fluid parameter was intensified. Therefore, the Burger fluid velocity was lower for the Burger fluid parameter $\beta_2$. The graphical relation between Deborah number $\beta_3$ and Burger nanofluid velocity for both the stretching sheet ($\gamma = 0$) and cylinder ($\gamma > 0$) was discussed in Figure 7. In this, the increment in Burger nanofluid velocity for both stretching sheet ($\gamma = 0$) and cylinder ($\gamma > 0$) is noticed against larger values of Deborah number $\beta_3$. The flow's creep phenomena were manifested by the retardation time. The burger fluid velocity increased due to the retardation time in the fluid motion which was the time required for achieving shear stress. The shear stress of the burger nanofluid is larger with the enchantment of Deborah number $\beta_3$ which increased the velocity of the Burger fluid.

## 6.3 Temperature profile

Figures 8–10 explain the influence of dimensionless heat generation parameter $\delta$, Biot number Bi, and Prandtl number Pr on the Burger nanofluid temperature profile $\theta(\xi)$ for both stretching sheet ($\gamma = 0$) and cylinder ($\gamma > 0$). Figure 8 was constructed for the variation of Burger nanofluid temperature against heat generation parameter $\delta$ for both the stretching sheet ($\gamma = 0$) and cylinder ($\gamma > 0$). From this investigation, it was clear that the enhancing estimations of heat generation parameter $\delta$ amplified the

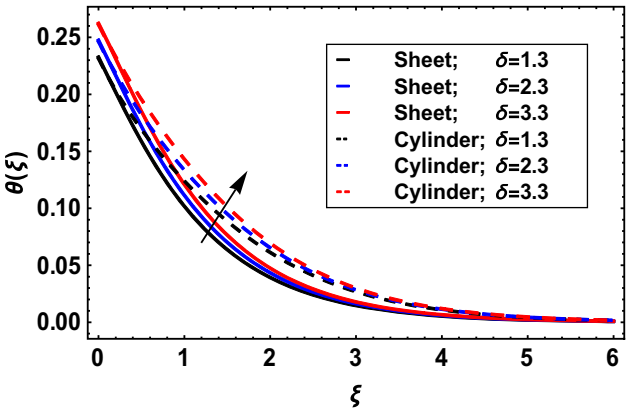


**Figure 8:** Change in nanofluid temperature due to $\delta$.

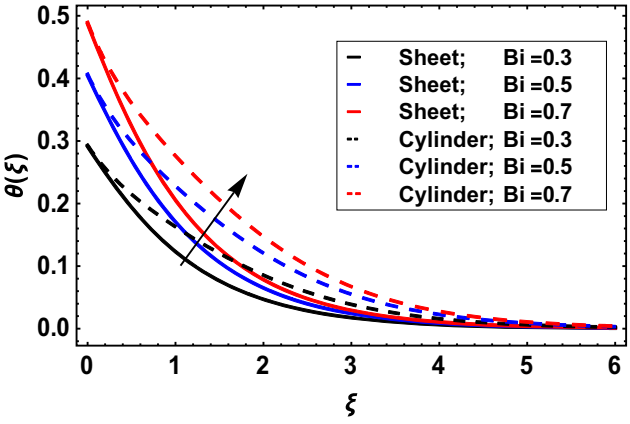


**Figure 9:** Change in nanofluid temperature due to Bi.

temperature of the Burger nanofluid for both the stretching sheet ($\gamma = 0$) and cylinder ($\gamma > 0$). The reason was that the enhancement in heat generation parameter $\delta$ produced an additional amount of heat which augments the heat transmission feature of the flow system. That's why the Burger fluid temperature becomes higher. Figure 9 explored the variation of Burger nanofluid temperature for growing values of thermal Biot number Bi for both stretching sheet ($\gamma = 0$) and cylinder ($\gamma > 0$). From this inquiry, it was examined that the temperature of the Burger nanoliquid was improved for both stretching sheet ($\gamma = 0$) and cylinder ($\gamma > 0$) with the enrichment of Bi. It was noticed that inside the fluid particles, the resistance of heat transport boost-up for both stretching sheet ($\gamma = 0$) and cylinder ($\gamma > 0$) when the thermal Biot number heightens. Furthermore, at the surface of the body, the rate of heat transport was decayed but the convection coefficient was increased. Then a lot of extra amounts of heat were transferred from the surface of the cylinder to the fluid particles that enhanced the fluid temperature. The change in the

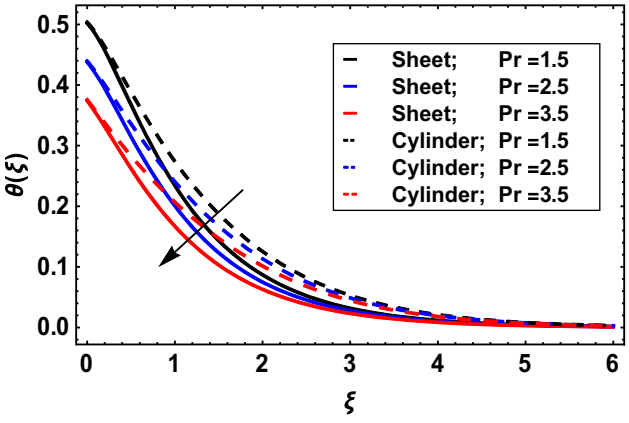


**Figure 10:** Change in nanofluid temperature due to Pr.

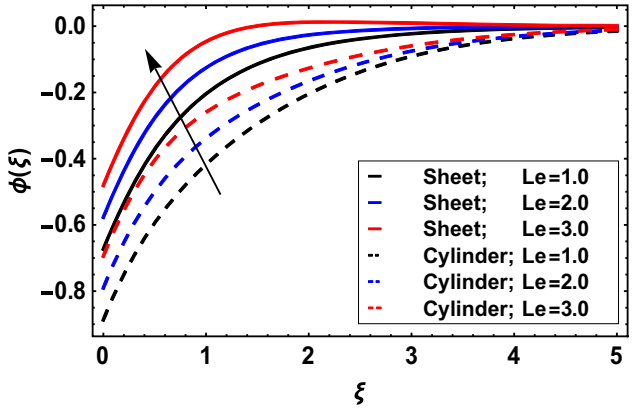


**Figure 11:** Change in nanofluid concentration due to Le.

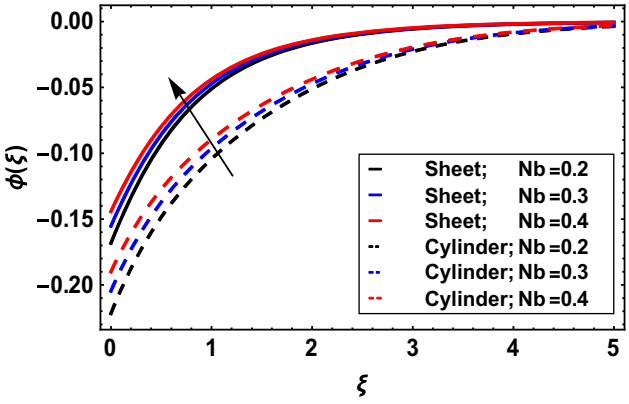


**Figure 12:** Change in nanofluid concentration due to Nb.

temperature of Burger nanofluid for higher estimation of Prandtl number Pr for both stretching sheet ($\gamma = 0$) and cylinder ($\gamma > 0$) was studied in Figure 10. From this, it was remarked that the decrement in Burger nanofluid temperature was inspected for the rising estimation of Prandtl number for both stretching sheet ($\gamma = 0$) and cylinder ($\gamma > 0$). Physically, the thermal diffusivity of the fluid was decayed due to the enhancement of Prandtl number because Prandtl number and thermal diffusivity were inversely proportional. That's why the boundary layer thickness and fluid temperature were weaker.

### 6.4 Concentration profile

The consequence of Lewis number Le, Brownian motion parameter Nb, and thermophoresis parameter Nt on the concentration profile $\phi(\xi)$ for both stretching sheet ($\gamma = 0$) and cylinder ($\gamma > 0$) is elaborated in Figures 11–13. The significance of Lewis number Le for both stretching sheet ($\gamma = 0$) and cylinder ($\gamma > 0$) on the concentration of Burger nanofluid was intended in Figure 11. From this review, it was detected that the elevation in the concentration of Burger nanofluid was observed for increasing values of Lewis number Le for both the stretching sheet ($\gamma = 0$) and cylinder ($\gamma > 0$). The graph of Burger nanofluid concentration for both stretching sheet ($\gamma = 0$) and cylinder ($\gamma > 0$) against the rising estimation of Nb was deliberated in Figure 12. The heightening impact of the concentration of Burger nanofluid for both stretching sheet ($\gamma = 0$) and cylinder ($\gamma > 0$) was distinguished for intensifying the estimation Nb. Figure 13 explained the significance of Nt on the concentration of Burger nanofluid for both the stretching sheet ($\gamma = 0$) and cylinder ($\gamma > 0$). From this, it was clear that the Burger nanofluid concentration decayed for both the stretching sheet ($\gamma = 0$) and cylinder ($\gamma > 0$) for escalating values of the thermophoresis parameter Nt.

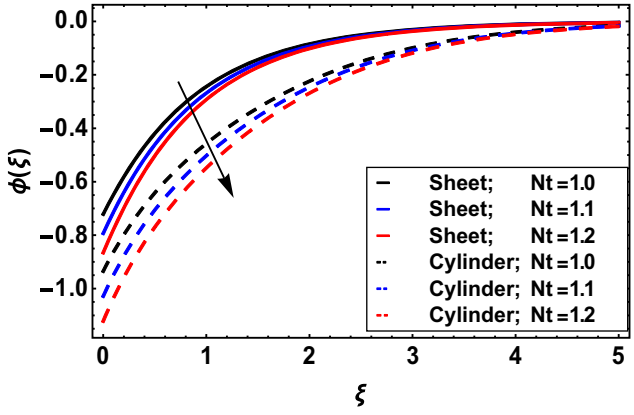


**Figure 13:** Change in nanofluid concentration due to Nt.

## 7 Conclusion

In this study, the Burger nanofluid problem in the presence of convective heat and mass transport phenomena for both stretching sheet and cylinder was addressed. The heat source/sink effects were applied in the temperature equation for the investigation of the temperature field of the Burger nanofluid. By applying the HAM on the higher order nonlinear ODEs, the analytical resolution of this study was attained. Finally, the outcomes of numerous flow parameters were calculated and debated in detail. The key findings of the present analysis were

- The Nusselt number was enhanced for both the stretching sheet and cylinder with the augmentation of the Biot number.
- The declining performance in the Nusselt number was observed for intensifying the estimation of heat generation parameters for both the stretching sheet and cylinder.

- The Burger nanofluid velocity was amplified for both stretching sheet and cylinder with the heightening of Deborah number.
- For both the stretching sheet and cylinder, the higher estimation of heat generation parameter, Biot number, and Prandtl number enhanced the temperature of the Burger nanofluid.
- Intensification in Burger nanofluid concentration is noted against the expanding values of Lewis number and Brownian motion parameter for both stretching sheet and cylinder.
- For both stretching sheet and cylinder, the Burger fluid concentration is lower for thermophoresis parameter.

**Funding information:** The authors acknowledge the financial support provided by the Center of Excellence in Theoretical and Computational Science (TaCS-CoE), KMUTT. Moreover, this research project is supported by Thailand Science Research and Innovation (TSRI) Basic Research Fund: Fiscal year 2022 (FF65).

**Author contributions:** All authors have accepted responsibility for the entire content of this manuscript and approved its submission.

**Conflict of interest:** The authors state no conflict of interest.

# References

[1] Khan AA, Abbas N, Nadeem S, Shi QH, Malik MY, Ashraf M, et al. Non-Newtonian based micropolar fluid flow over nonlinear starching cylinder under Soret and Dufour numbers effects. Int Commun Heat Mass Transf. 2021;127:105571.

[2] Bilal M, Urva Y. Analysis of non-Newtonian fluid flow over fine rotating thin needle for variable viscosity and activation energy. Archive Appl Mech. 2021;91(3):1079–95.

[3] Ramzan M, Khan NS, Kumam P. Mechanical analysis of non-Newtonian nanofluid past a thin needle with dipole effect and entropic characteristics. Sci Rep. 2021;11(1):1–25.

[4] Alhadhrami A, Vishalakshi CS, Prasanna BM, Sreenivasa BR, Alzahrani HA, Gowda RP, et al. Numerical simulation of local thermal non-equilibrium effects on the flow and heat transfer of non-Newtonian Casson fluid in a porous media. Case Stud Therm Eng. 2021;28:101483.

[5] Mallawi FOM, Eswaramoorthi S, Sivasankaran S, Bhuvaneswari M. Impact of stratifications and chemical reaction on convection of a non-Newtonian fluid in a Riga plate with thermal radiation and Cattaneo-Christov flux. J Therm Anal Calorim. 2021;1–17.

[6] Dawar A, Shah Z, Tassaddiq A, Kumam P, Islam S, Khan W. A convective flow of williamson nanofluid through cone and wedge with non-isothermal and non-isosolutal conditions: a revised buongiorno model. Case Stud Therm Eng. 2021;24:100869.

[7] Reddy MV, Lakshminarayana P. Cross-diffusion and heat source effects on a three-dimensional MHD flow of Maxwell nanofluid over a stretching surface with chemical reaction. Eur Phys J Spec Top. 2021;230:1–9.

[8] Qaiser D, Zheng Z, Khan MR. Numerical assessment of mixed convection flow of Walters-B nanofluid over a stretching surface with Newtonian heating and mass transfer. Therm Sci Eng Prog. 2021;22:100801.

[9] Hiba B, Redouane F, Jamshed W, Saleel CA, Devi SSU, Prakash M, et al. A novel case study of thermal and streamline analysis in a grooved enclosure filled with (Ag–MgO/Water) hybrid nanofluid: Galerkin FEM. Case Stud Therm Eng. 2021;28:101372.

[10] Ouni M, Ladhar LM, Omri M, Jamshed W, Eid MR. Solar water-pump thermal analysis utilizing copper–gold/engine oil hybrid nanofluid flowing in parabolic trough solar collector: Thermal case study. Case Stud Therm Eng. 2022;30:101756.

[11] Khan U, Bouslimi J, Zaib A, Al-Mubaddel FS, Imtiaz N, Alharbi AN, et al. MHD 3D crossflow in the streamwise direction induced by nanofluid using Koo–Kleinstreuer and Li (KLL) correlation. Coatings. 2021;11(12):1472.

[12] Bejawada SG, Jamshed W, Safdar R, Reddy YD, Alanazi M, Zahran HY, et al. Chemical reactive and viscous dissipative flow of magneto nanofluid via natural convection by employing galerkin finite element technique. Coatings. 2022;12(2):151.

[13] Jamshed W, Prakash M, Devi S, Ibrahim RW, Shahzad F, Nisar KS, et al. A brief comparative examination of tangent hyperbolic hybrid nanofluid through a extending surface: numerical Keller–Box scheme. Sci Rep. 2021;11(1):1–32.

[14] Redouane F, Jamshed W, Devi S, Amine BM, Safdar R, Al-Farhany K, et al. Influence of entropy on Brinkman–Forchheimer model of MHD hybrid nanofluid flowing in enclosure containing rotating cylinder and undulating porous stratum. Sci Rep. 2021;11(1):1–26.

[15] Waqas H, Yasmin S, Muhammad T, Imran M. Flow and heat transfer of nanofluid over a permeable cylinder with nonlinear thermal radiation. J Mater Res Technol. 2021;14:2579–85.

[16] Hayat T, Ullah H, Ahmad B, Alhodaly MS. Heat transfer analysis in convective flow of Jeffrey nanofluid by vertical stretchable cylinder. Int Commun Heat Mass Transf. 2021;120:104965.

[17] Siddiqui BK, Batool S, Ul Hassan QM, Malik MY. Irreversibility analysis in the boundary layer MHD two dimensional flow of Maxwell nanofluid over a melting surface. Ain Shams Eng J. 2021;12:3217–27.

[18] Awan SE, Raja MAZ, Gul F, Khan ZA, Mehmood A, Shoaib M. Numerical computing paradigm for investigation of micropolar nanofluid flow between parallel plates system with impact of electrical MHD and Hall current. Arab J Sci Eng. 2021;46(1):645–62.

[19] Ramesh GK, Roopa GS, Rauf A, Shehzad SA, Abbasi FM. Time-dependent squeezing flow of Casson-micropolar nanofluid with injection/suction and slip effects. Int Commun Heat Mass Transf. 2021;126:105470.

[20] Lv YP, Gul H, Ramzan M, Chung JD, Bilal M. Bioconvective Reiner–Rivlin nanofluid flow over a rotating disk with

Cattaneo–Christov flow heat flux and entropy generation analysis. Sci Rep. 2021;11(1):1–18.
[21] Waqas H, Farooq U, Alqarni MS, Muhammad T. Numerical investigation for 3D bioconvection flow of Carreau nanofluid with heat source/sink and motile microorganisms. Alex Eng J. 2021;61(3):2366–75.
[22] Kumar R, Kumar R, Sharma T, Sheikholeslami M. Mathematical modeling of stagnation region nanofluid flow through Darcy–Forchheimer space taking into account inconsistent heat source/sink. J Appl Math Comput. 2021;65(1):713–34.
[23] El-Shorbagy MA, Algehyne EA, Ibrahim M, Ali V, Kalbasi R. Effect of fin thickness on mixed convection of hybrid nanofluid exposed to magnetic field-Enhancement of heat sink efficiency. Case Stud Therm Eng. 2021;26:101037.
[24] Ibrahim M, Algehyne EA, Saeed T, Berrouk AS, Chu YM, Cheraghian G. Assessment of economic, thermal and hydraulic performances a corrugated helical heat exchanger filled with non-Newtonian nanofluid. Sci Rep. 2021;11(1):1–16.
[25] Mahmoud EE, Algehyne EA, Alqarni MM, Afzal A, Ibrahim M. Investigating the thermal efficiency and pressure drop of a nanofluid within a micro heat sink with a new circular design used to cool electronic equipment. Chem Eng Commun. 2021;1–13.
[26] Shah NA, Animasaun IL, Chung JD, Wakif A, Alao FI, Raju CSK. Significance of nanoparticle's radius, heat flux due to concentration gradient, and mass flux due to temperature gradient: the case of Water conveying copper nanoparticles. Sci Rep. 2021;11(1):1–11.
[27] Wakif A, Animasaun IL, Khan U, Alshehri AM. Insights into the gen1eralized Fourier's and Fick's laws for simulating mixed bioconvective flows of radiative-reactive walters-b fluids conveying tiny particles subject to Lorentz force. 2021.
[28] Shafiq A, Rasool G, Alotaibi H, Aljohani HM, Wakif A, Khan I, et al. Thermally enhanced Darcy–Forchheimer Casson-water/glycerine rotating nanofluid flow with uniform magnetic field. Micromachines. 2021;12(6):605.
[29] Wakif A, Chamkha A, Animasaun IL, Zaydan M, Waqas H, Sehaqui R. Novel physical insights into the thermodynamic irreversibilities within dissipative EMHD fluid flows past over a moving horizontal riga plate in the coexistence of wall suction and joule heating effects: a comprehensive numerical investigation. Arab J Sci Eng. 2020;45(11):9423–38.
[30] Wakif A. A novel numerical procedure for simulating steady MHD convective flows of radiative Casson fluids over a horizontal stretching sheet with irregular geometry under the combined influence of temperature-dependent viscosity and thermal conductivity. Math Probl Eng. 2020;2020:1–20.
[31] Wakif A, Animasaun IL, Khan U, Shah NA, Thumma T. Dynamics of radiative-reactive Walters-b fluid due to mixed convection conveying gyrotactic microorganisms, tiny particles experience haphazard motion, thermo-migration, and Lorentz force. Phys Scr. 2021;96(12):125239.
[32] Khashi'ie NS, Arifin NM, Pop I. Magnetohydrodynamics (MHD) boundary layer flow of hybrid nanofluid over a moving plate with Joule heating. Alex Eng J. 2021;11:14128.
[33] Krishna MV, Ahammad NA, Chamkha AJ. Radiative MHD flow of Casson hybrid nanofluid over an infinite exponentially accelerated vertical porous surface. Case Stud Therm Eng. 2021;27:101229.
[34] Haider SMA, Ali B, Wang Q, Zhao C. Stefan blowing impacts on unsteady mhd flow of nanofluid over a stretching sheet with electric field, thermal radiation and activation energy. Coatings. 2021;11(9):1048.
[35] Ahmed K, Akbar T, Muhammad T, Alghamdi M. Heat transfer characteristics of MHD flow of Williamson nanofluid over an exponential permeable stretching curved surface with variable thermal conductivity. Case Stud Therm Eng. 2021;28:101544.
[36] Tassaddiq A. Impact of Cattaneo-Christov heat flux model on MHD hybrid nano-micropolar fluid flow and heat transfer with viscous and joule dissipation effects. Sci Rep. 2021;11(1):1–14.
[37] Qayyum S, Hayat T, Shehzad SA, Alsaedi A. Effect of a chemical reaction on magnetohydrodynamic (MHD) stagnation point flow of Walters-B nanofluid with Newtonian heat and mass conditions. Nucl Eng Technol. 2017;49(8):1636–44.
[38] Ghasemi SE, Hatami M. Solar radiation effects on MHD stagnation point flow and heat transfer of a nanofluid over a stretching sheet. Case Stud Therm Eng. 2021;25:100898–1004.
[39] Ramzan M, Kumam P, Nisar KS, Khan I, Jamshed W. A numerical study of chemical reaction in a nanofluid flow due to rotating disk in the presence of magnetic field. Sci Rep. 2021;11:19399.
[40] Awais M, Awan SE, Raja MAZ, Parveen N, Khan WU, Malik MY, et al. Effects of variable transport properties on heat and mass transfer in MHD bioconvective nanofluid rheology with gyrotactic microorganisms: numerical approach. Coatings. 2021;11(2):231.
[41] Srinivasulu T, Goud BS. Effect of inclined magnetic field on flow, heat and mass transfer of Williamson nanofluid over a stretching sheet. Case Stud Therm Eng. 2021;23:100819.
[42] Zeeshan A, Majeed A, Akram MJ, Alzahrani F. Numerical investigation of MHD radiative heat and mass transfer of nanofluid flow towards a vertical wavy surface with viscous dissipation and Joule heating effects using Keller-box method. Math Comput Simul. 2021;190:1080–109.
[43] Punith Gowda RJ, Naveen Kumar R, Jyothi AM, Prasannakumara BC, Sarris IE. Impact of binary chemical reaction and activation energy on heat and mass transfer of marangoni driven boundary layer flow of a non-Newtonian nanofluid. Processes. 2021;9(4):702.
[44] Shi QH, Khan MN, Abbas N, Khan MI, Alzahrani F. Heat and mass transfer analysis in the MHD flow of radiative Maxwell nanofluid with non-uniform heat source/sink. Waves Random Complex Media. 2021;1–24.
[45] Zhao T, Khan MR, Chu Y, Issakhov A, Ali R, Khan S. Entropy generation approach with heat and mass transfer in magnetohydrodynamic stagnation point flow of a tangent hyperbolic nanofluid. Appl Math Mech. 2021;42(8):1205–18.
[46] Arif M, Kumam P, Kumam W, Khan I, Ramzan M. A fractional model of casson fluid with ramped wall temperature: engineering applications of engine oil. Comput Math Methods. 2021;3:e1162.
[47] Rasool G, Shafiq A, Alqarni MS, Wakif A, Khan I, Bhutta MS. Numerical scrutinization of Darcy–Forchheimer relation in convective magnetohydrodynamic nanofluid flow bounded by nonlinear stretching surface in the perspective of heat and mass transfer. Micromachines. 2021;12(4):374.

[48] Wakif A, Boulahia Z, Sehaqui R. A semi-analytical analysis of electro-thermo-hydrodynamic stability in dielectric nanofluids using Buongiorno's mathematical model together with more realistic boundary conditions. Results Phys. 2018;9:1438–54.
[49] Hayat T, Waqas M, Shehzad SA, Alsaedi A. Mixed convection flow of a Burgers nanofluid in the presence of stratifications and heat generation/absorption. Eur Phys J Plus. 2016;131(8):1–11.
[50] Khan M, Iqbal Z, Ahmed A. Stagnation point flow of magnetized Burgers' nanofluid subject to thermal radiation. Appl Nanosci. 2020;10(12):5233–46.
[51] Khan M, Iqbal Z, Ahmed A. A mathematical model to examine the heat transport features in Burgers fluid flow due to stretching cylinder. J Therm Anal Calorim. 2020;1–15.
[52] Mabood F, Khan WA, Ismail AM. MHD boundary layer flow and heat transfer of nanofluids over a nonlinear stretching sheet: a numerical study. J Magnetism Magnetic Mater. 2015;374:569–76.
[53] Wang CY. Free convection on a vertical stretching surface. ZAMM-J Appl Math Mechanics/Z Angew Math Mechanik. 1989;69(11):418–20.
[54] Khan WA, Pop I. Boundary-layer flow of a nanofluid past a stretching sheet. Int J Heat Mass Transf. 2010;53(11–12):2477–83.
[55] Salahuddin T, Hussain A, Malik MY, Awais M, Khan M. Carreau nanofluid impinging over a stretching cylinder with generalized slip effects: using finite difference scheme. Results Phys. 2017;7:3090–9.